Modeling of the Optical Behavior of Myocardial Fibers in Polarized Light Imaging

Paul Audain Desrosiers[1,2], Gabrielle Michalowicz[1], Pierre-Simon Jouk[1], Yves Usson[1], and Yuemin Zhu[2]

[1] CNRS, UMR 5525, Université Joseph Fourier de Grenoble
[2] CREATIS, CNRS UMR 5220, INSERM U1044, INSA de Lyon, Université de Lyon, Villeurbanne

Abstract. Many cardiovascular diseases are linked to anomalies in myocardial fibers. The purpose of this paper is to model the birefringence of myocardial fibers in polarized light imaging (PLI) with future application to measurements on real myocardial tissues. The method consists in modeling the behavior of a uni-axial birefringent crystal by means of the Muller matrix, and measuring the final intensity of polarized light and consequently the orientation of myocardial fibers, by using crossed polarizers. The method was illustrated with a tissue modeled as a volume of $100\times100\times500\mu m^3$. This volume was divided into cubes of size $20\mu m$ close to cell diameter. The fiber orientation within the cube was defined by azimuth and elevation angles. The results showed that the proposed modeling enables us to find the optimal conditions for the PLI of 3D fiber orientations and design a model for the myocardial tissue measurement from PLI.

Keywords: myocardial fibers, fiber architecture, human heart, fiber orientation, polarizers, polarized light.

1 Introduction

Cardiovascular disease is the first cause of mortality in the world. According to the OMS in 2030 the number of death will reach more than 17.3 million. Disorders in the heart being linked to myocardial fibers, many studies have tried to understand the architecture of myocardial fibers in the ventricular mass. Some old techniques used fiber peeling of the heart from pericardium to endocardium. Mac Callum (1900) peeled the heart of the pig and human in order to study the fibers structure. Other techniques were dissection methods, such as those of Mall [1], Robb [2], and Torrent-Guasp [3], while Hort [4] and Streeter [5] developed histological methods. More recent imaging techniques include diffusion tensor magnetic resonance imaging (DT-MRI or DTI) [6], [7], [8], [9] and microscopic techniques using the polarized light imaging (PLI) have been developed. The use of polarized light has been introduced in biology since the end of the 19th century as a method for studying the structure of the human tissue. The authors of [10] used the polarized light to study the light scattering in Bacillus subtilis. PLI was also

O. Camara et al. (Eds.): STACOM 2012, LNCS 7746, pp. 235–244, 2013.

used to visualize superficial layers of tissue where cancer arises in the skin [11], to analyze the healing after myocardial infarction [12], to establish the cartography of the pattern of myofibres in the second trimester fetal human heart [13], to study the architecture of the ventricle during fetal and neonatal life [14], to make an analysis of the collagen network [15], to investigate the topography of myocardial cells during embryonic and fetal life development [16], and to characterize the myocardium, including healthy, infarcted, and stem-cell-regeneration tissues using polarized light [17]. We used polarized light for many years in order to extract information in heart in neonatal life. In prior works on cot death, we analyzed the structure of autopsied hearts in the selected region such as the apex, the right ventricle and the left ventricle using polarized light, and have been able to observe the presence of heterogeneity of myocardial cells with a confocal microscopy [18]. However with the confocal microscopy, only a small and two-dimensional region was observed. More generally speaking, only PLI provides a very robust angular accuracy and 3D orientation map of myocardial cells with a high spatial resolution 0.1mm×0.1mm×0.5mm. Also PLI does not involve any human operation during the measurement process. However PLI cannot be used on the living human heart. Meanwhile, Some other techniques like DT-MRI or DTI can be used on the living human heart, but are limited in spatial resolution. On the other hand, although many researches were reported that are focused on the orientation of the myocardial fibers in polarized light, there is not yet work that addresses the degree of homogeneity of myocardial fibers.

In this paper, we propose to model the behavior of myocardial fibers in polarized light under controlled condition, and investigate the degree of homogeneity of the myocardial cells.

2 Materials and Methods

2.1 Sample Preparation

After removing the heart from the thorax, the hearts were perfused and fixed in a solution of 4% neutral buffered formaldehyde, and then immersed for 1 week in the same condition. The ventricles were then removed by severing the atria 1 mm proximal to the auriculo-ventricular groove and the great vessels of 3 mm from the ventricle. The ventricles were embedded in a resin of methyl methacrylate (MMA) using a protocol [16]. The specimens were infiltrated under vacuum (10 mbar) at room temperature in a series of mixtures of glycol methacrylate (GMA) and MMA in which the concentration of MMA was gradually increased to obtain pur MMA. The heart was then embedded by polymerization of MMA at 25° C. After polymerization, the heart was clearly seen through the transparent resin. It can be oriented according to the prerequisite referential system : coronal transversal, or sagittal. This was done by polishing the base of the block, which was mounted on the saw stage and determines the plane of serial sectioning, and a series of thick sections (500 μm) were cut with a diamond wire saw. The rate of penetration of the rotatory saw was set to a low speed (one hour per section) in order to avoid mechanical stress and distortions. By canceling the

optical properties of the collagen network, MMA embedding guarantee that PLI information was only due to the orientation of the myocardial cells [18].

To study fiber orientation with polarized light, an experimental PLI system was designed and constructed using the following elements:

a) A light source (unpolarized light i.e. the electric field E vibrating in all directions).
b) A linear polarizer whose vibration axis vibrates parallel to the West-East position, with reference to the stage of the virtual optic bench.
c) The birefringent sample to be tested.
d) A second linear polarizer whose vibration axis is perpendicular to the vibrating axis of the first polarizer.
e) A CCD camera that records the amount of transmitted light.

The optical bench was controlled and monitored by software we developed in C/C++. Light is an electromagnetic wave; the electric field vector E vibrates perpendicular to the direction along which it propagates. The light beam is composed of waves whose vibration axes are randomly distributed. The polarizer is an optical part which selects a specific vibration direction of the light. When the vibration axes of two polarizers are perpendicular to each other, without any birefringent sample between them, the light is blocked and the amplitude of light is down to zero. When a birefringent sample is rotated between crossed polarizers, it interferes with the light vibrating axis, and some light is transmitted across the second polarizer.

2.2 Optical Element Modeling

Thus, the amount of transmitted light is a function of the birefringence of the sample, and this birefringence is a function of the physico-chemical characteristics of the sample and its orientation with respect to the light. The myocardial birefringence is due to different molecules : the myosin that behaves like uni-axial positive birefringent crystal, and collagen that creates a structural birefringence. In order to collect the myosin birefringence signal alone, we cancel out the collagen structure birefringence, the biological sample was embedded in MMA whose refractive index is the same as that of collagen. When a polarizer beam crosses a uni-axial birefringent sample, the ray is divided in two beams (ordinary and extraordinary) that vibrate perpendicular to each other with a difference of phase that depends on the structural properties of the sample [19]. The birefringence (n_o-n_e) of the uni-axial sample was measured as the difference of refraction indices of the ordinary ray n_o and the extraordinary ray n_e.

In order to model the optic parts of the above-mentioned PLI system, we used the Muller matrix, which was initially proposed by Hans Muller in 1940 for representing any optic element by a 4×4 matrix [20]. The Muller matrix is based on Stokes' parameters. The light can be described by four parameters, the first one is the total intensity of the light and the three others describe the polarization state. If we know the Stokes' parameters in $S_{(in)}$ and Stokes' parameters out $S_{(out)}$ of an optic part, the Muller matrix is expressed as

$$S_{(out)} = MS_{(in)}. \tag{1}$$

So, each element can be represented by a specific Muller matrix as follows.

$$\begin{pmatrix} S'_0 \\ S'_1 \\ S'_2 \\ S'_3 \end{pmatrix} = \begin{pmatrix} m_{00}\ m_{01}\ m_{02}\ m_{03} \\ m_{10}\ m_{11}\ m_{12}\ m_{13} \\ m_{20}\ m_{21}\ m_{22}\ m_{23} \\ m_{30}\ m_{31}\ m_{32}\ m_{33} \end{pmatrix} \begin{pmatrix} S_0 \\ S_1 \\ S_2 \\ S_3 \end{pmatrix} \tag{2}$$

The Muller matrix M_d for the depolarizer which insures that the light is not polarized, can be written as

$$M_d = \begin{pmatrix} 1\ 0\ 0\ 0 \\ 0\ 0\ 0\ 0 \\ 0\ 0\ 0\ 0 \\ 0\ 0\ 0\ 0 \end{pmatrix} \tag{3}$$

where $M_d(1,1)$ represents the amplitude of unpolarized light.

The Muller matrix M_p for the polarizers is characterized by α the rotation angle about the z-axis. It can be expressed as

$$M_p = \frac{1}{2} \begin{pmatrix} 1 & cos2\alpha & sin2\alpha & 0 \\ cos2\alpha & cos^2 2\alpha & cos2\alpha sin2\alpha & 0 \\ sin2\alpha & cos2\alpha sin2\alpha & sin^2 2\alpha & 0 \\ 0 & 0 & 0 & 0 \end{pmatrix} \tag{4}$$

The uni-axial birefringent sample is represented as a stack rotator and phase shifter

$$M_s = M(2\theta)M(\varphi(\Phi)). \tag{5}$$

The phase $\varphi(\Phi)$ of the birefringent sample depends on the birefringence (n_o-n_e), the wavelength λ, the thickness e of the sample, and the elevation angle Φ. Therefore, the ellipticity state ε of the sample represents the polarization degree of the light; it varies from $0<\varepsilon<1$. Empirically, the uni-axial birefringent of the sample can be represented by

$$M_s = \begin{pmatrix} 1 & 0 & 0 & 0 \\ 0 & d^2 - e^2 - f^2 + g^2 & 2(de + fg) & 2(df + eg) \\ 0 & 2(de - fg) & -d^2 + e^2 - f^2 + g^2 & -2(dg - ef) \\ 0 & 2(df - eg) & 2(dg + ef) & -d^2 - e^2 + f^2 + g^2 \end{pmatrix} \tag{6}$$

$d = \cos(2\varepsilon)\cos(2\theta)\sin(\varphi/2)$
$e = \cos(2\varepsilon)\sin(2\theta)\sin(\varphi/2)$
$f = \sin(2\varepsilon)\cos(2\theta)\sin(\varphi/2)$
$g = \cos(\varphi/2)$

with

$$\varphi(\Phi) = \frac{2\pi}{\lambda}(n_o - n_e)e. \tag{7}$$

and

$$(n_o - n_e) = 1.5 \left(\frac{1}{\sqrt{1 - \frac{2(n_o - n_e)_{max} \cos^2 \Phi}{1.5}}} - 1 \right) \tag{8}$$

where
φ = phase shift
λ = wavelength of light
e = thickness of the sample
n_o-n_e = birefringence of the sample
α = rotation angle of the polarizers
θ = azimuth angle
Φ = elevation angle
ϵ = Ellipticity (flattening measure of the ellipse).

After calculating the Muller matrix of each optic part, equation 9 was used to simulate the behavior of the uni-axial birefringent sample in optical bench, so all our simulation were run with GNU/Octave.

3 Results and Discussion

Based on the above modeling based on optical laws, we are now able to infer the mean spatial orientation of the myosin filaments for each pixel of the section. This orientation in space can be described by means of two angles : the azimuth and elevation angles. The azimuth angle is the angle between the west-east axis of the stage (x-axis) and the projection of the uni-axial sample direction on the stage plane, and the elevation angle corresponds to the obliquity of the uni-axial sample with respect to the plane of the section.

3.1 Light Amplitude Variation with Elevation or Azimuth Angle

The two polarizers were rotated at the same time. The first polarizer angle α_1 is rotated from 0° to 90° and the second polarizer angle α_2 is rotated from α_1+90° (so forming two crossed polarizers) with the uni-axial birefringent sample (ϵ= 0.02) between them. Figure 1a shows how the amplitude of the light varies with elevation angle for a given azimuth angle (45°). Note that The amplitude of 1.0 corresponds to the initial amplitude of the depolarized light source. Each curve corresponds to an elevation angle Φ (from 0° to 90°) of the birefringent sample. All the curves pass through the same corresponding point, that is the 45° point. At 45°, the amplitude of the light is dropped to zero, no light coming out of the second polarizer. That means, at this point, the azimuth angle θ is not depending on the rest of the system. The mathematical expression of amplitude of the polarized light in the setup is

$$M(1,1) = M_{p1}(\alpha_1) M_s(\theta, \varphi(\Phi)) M_{p1}(\alpha_2). \tag{9}$$

M(1,1) : represents the amplitude of the light in the system.

From the simulation based on the physical equation 9, we deduced a phenomenological model, that can be expressed as

$$y(\alpha) = Bcos\left(2\left(\alpha + \frac{\pi}{4} - \theta\right)\right)^2 \tag{10}$$

Least squares method allowed to fit the phenomenological model, that means the equation 10 with the curves of figure 1a, 1b (fitting at 99%) which come from the physical equation 9. In turn, equation 10 was used to extract the real parameter of the system under polarized light, such as the amplitude of the light, and the orientation of the myocardial cell.

where

B : represents the amplitude of the light (which depends on the elevation and the homogeneity)

θ : the azimuth angle of the birefringent sample

α :the rotation angle of the linear polarizer couple.

In Figure 1b, we represent the variation of the azimuth angle θ of the uniaxial birefringent sample ($\epsilon = 0.02$) from 0° to 180° (with a 20° step) with an elevation angle Φ set to a fixed value (0°). In this figure, all the curves have the same behavior except a phase shift that depends on the corresponding azimuth angle θ.

Note that all the curves are modulo 90° about azimuth angle. Moreover, all the curves dropped to zeros at their corresponding azimuth angle θ. For example, for an azimuth of 0°, the corresponding curve passes through its maximum at 45°.

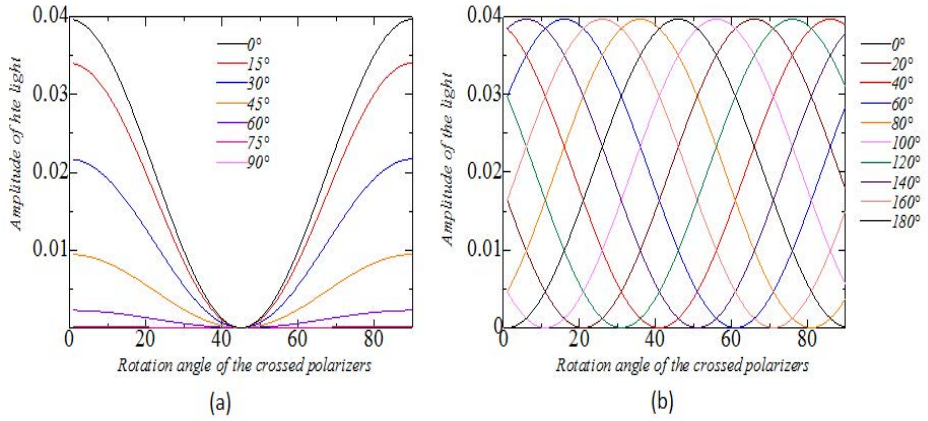

Fig. 1. a) Variation of the light amplitude as a function of rotation angles of the two polarizers when varying elevation angles and fixing azimuth angle; b) Variation of the light amplitude as a function of rotation angles of the two polarizers when varying azimuth angles and fixing elevation angle

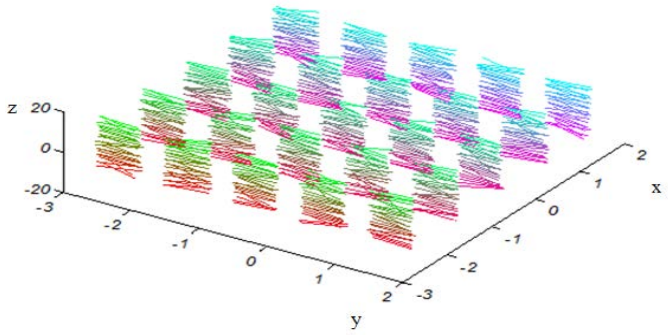

Fig. 2. Simulated volume with fibers having a dispersion angle of 15°, each vector is shown with a color of its own

3.2 Tissue Element of $100\times100\times500\mu m^3$

After simulating the behavior of a uni-axial birefringent sample, we now apply the same modeling method to a simulated tissue which was modeled as a mixture of small uni-axial birefringent elements. The tissue was modeled as a volume of $100\times100\times500\mu m^3$, which is divided into 25 cubic elements, each of which is formed of 25 cells (of 20 μm). For each cubic element, we set the local 3D orientation (azimuth and elevation) such that various conditions are experienced: homogeneous volume (all fibers are parallels) and heterogeneous volume (with solid angular dispersion, as shown in figure 2). The solid angle defines the angle dispersion of fibers.

3.3 Homogeneity with Parallels Fibers

In this configuration, the volume is composed of perfectly parallel fibers, without any variability. We used equation 9 with the same condition, and the uni-axial birefringent sample was replaced by the volume. The azimuth angle θ of the volume was set to a fixed value (45°), with a variation of the elevation angle Φ from 0° to 90°. As expected, since the fibers run perfectly parallel and are homogeneous, the corresponding curves pass through a minimum value at 45°, and at this point the amplitude of the light is dropped to zero, which is consistent with the result shown in figure 1a.

We obtain here exactly the same results as those physically measured with the real optical bench [21].

3.4 Heterogeneity with Solid Angle Dispersion

In this configuration, cell direction variability has been added to the volume. The cell orientation of the myocardial fibers is normally distributed and centered, with a standard deviation σ (solid angle) of dispersion of 15° (figure 2). The azimuth angle θ is still set to a fixed value (45°) and the elevation angle Φ

is set to 0°. As the volume is not homogeneous, all the curves begin to detach (offset) from abscissas at 45° as far as the solid angle increases. Moreover the amplitude of the light is decreased, and different from zero at 45°. This light leakage in the second polarizer depends on the summation of the disorders of the myocardial fibers. So, this offset depends on the standard deviation of the myocardial fibers; this is a consequence of the usual dispersion of fibers orientation around the mean orientation. Since we introduced variability in a stochastic manner, the subsequent results are the statistical measurements obtained after the simulation of 10 data sets. In figure 3a, only one data set is shown. Figures 3b to 3c show, respectively, the variation of the amplitude of the light (parameter B), the variation of the azimuth angle (parameter θ), and the offset angle (parameter A) with an angular dispersion that varied from 0° to 40°. So, all these curves can be summarized by the following model

$$y(\alpha) = A + Bcos\left(2\left(\alpha + \frac{\pi}{4} - \theta\right)\right)^2 \tag{11}$$

A = offset which characterized the heterogeneity; B = estimates amplitude of the light that depends on both the elevation; θ = azimuth angle; α = rotation angle of the couple linear polarizer.

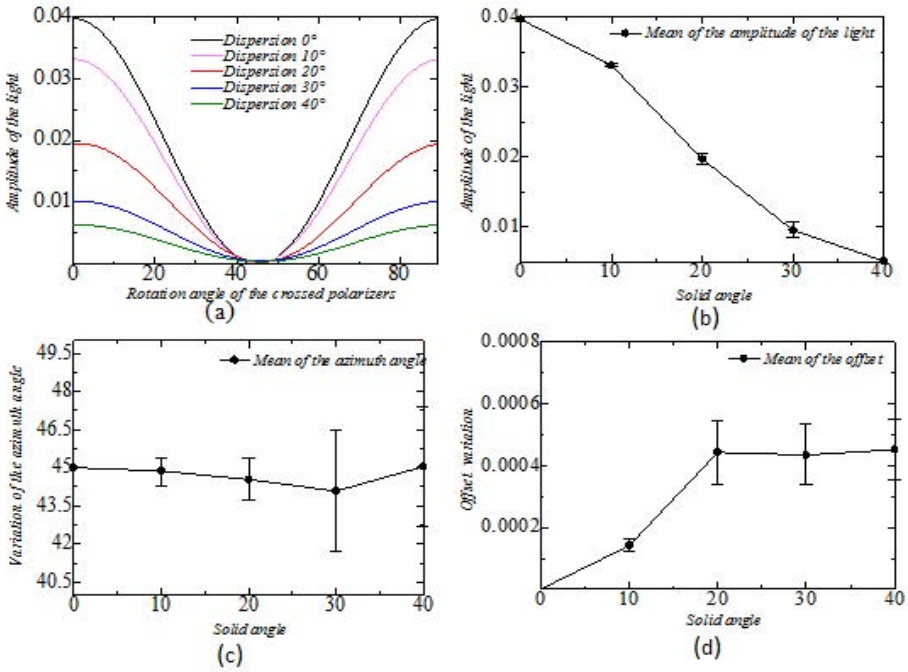

Fig. 3. Behavior of the volume in the presence of fiber angle dispersion (solid angle)

With the modeling results presented above, we can see that it is possible to predict the degree of homogeneity of the myocardial fibers with three parameters such as the amplitude of the light, weak variation of the azimuth angle, and the emergence of an offset.

4 Conclusion

The proposed PLI system modeling allowed us to understand the optical behavior of myocardial fibers in polarized light, and will help us to develop an adequate strategy to extract unambiguously the local 3D orientation (azimuth and elevation angles) on real myocardial tissues. We are working on applying the modeling to true human hearts in order to better physically measure the actual orientation of myocardial fibers.

Acknowledgements. Funding for this project was provided by a grant from the Région Rhône-Alpes France under the project CIBLE 2010.

References

1. Mall, F.P.: On the muscular architecture of the ventricles of the human heart. Am. J. Anat. 11, 211–266 (1911)
2. Robb, J.S., Robb, R.C.: The normal heart-anatomy and physiology of the structural units. Am. Heart J. 23, 455–467 (1942)
3. Torrent-Guasp, F.: Organizacion de la musculeta cardiaca ventricular. In: Zarco, P., Perez, J. (eds.) El Mecanico del Corazon, pp. 3–36. Ediciones toray, Barcelona (1975)
4. Hort, W.: Quantitative morphology and structural dynamics of the myocadium. Methods Achiev. Exp. Pathol. 5, 3–21 (1971)
5. Streeter Jr., D.D.: Gross morphology and fiber geometric of the heart. The Cardiovascular (1979)
6. Basser, P., Pierpaoli, C.: Microstructural and Physiological Features of Tissues Elucidated by Quantitative-diffusion-tensor MRI. J. Magn. Reson. Imaging 111(3), 209–219 (1996)
7. Wu, M.T., Tseng, W.Y., Su, M.Y., et al.: Diffusion Tensor Magnetic Resonance Imaging Mapping the Fiber Architecture Remodeling in Human Myocardium After Infarction. Circulation 114(10), 1036–1045 (2006)
8. Frindel, C., Robini, M., Schaerer, J., Croisille, P., Zhu, Y.M.: A graph-based approach for automatic cardiac tractography. MRM 64, 1215–1229 (2010)
9. Scmid, P., Jaermann, T., Boesiger, P., Niederer, P.F., Lunkenheimer, P.P., Cryer, C.W., Anderson, R.H.: Ventricular myocardial architecture as visualized in postmortem swine hearts using magnetic resonance diffusion tensor imaging. Eur. J. Cardiothorac. Surg. 27, 468–472 (2005)
10. Bickel, W.S., Davidson, J.F., Huffman, D.R., Kilkson, R.: Application of polarization effects in light scattering: a new biophysical tool. Proc. Natl. Acad. Sci. USA 73, 486–490 (1976)
11. Jacques, S.L., Roman, J.R., Lee, K.: Imaging Superficial Tissues With Polarized Light (2000)

12. Whittaker, P., Boughner, D.R., Kloner, R.A.: Analysis of Healing After Myocardial Infarction Using Polarized Light Microscopy (1989)
13. Jouk, P.-S., Usson, Y., Michalowicz, G., Grossi, L.: Three dimensional cartography of the pattern of the myofibres in the second trimester fetal human heart. Anat. Embriol. 202, 103–118 (2000)
14. Jouk, P.-S., Mourad, A., Misilic, V., Michalowicz, G., Raoul, A., Caillerie, D., Usson, Y.: Analysis of the fiber architecture of the heart by quantitative polarized light microscopy, accurancy, limitations and contribution to the study of the fiber architecture of the ventricles during fetal and neonatal life. Journal of Cardiothoracic Sugery, 916–922 (2007)
15. Rieppo, J., Hallikainen, J., Jurverlin, J.S., Kiviranta, I., Helminen, H.J., Hyttinen, M.M.: Practical considerations in use of polarized light microscopy in the analysis of the collage Network in cartilage. Microscopy Research and Technique 71, 279–287 (2008)
16. Jouk, P.-S., Brugal, G.: Etude de la topographie des cellules myocardiques au cours du développement embryonnaire et fœtal (1994)
17. Wood, M.F.G., et al.: Polarization birefringence measurement for characterizing the myocardium, including healthy, infarcted, and stem-cell-regeneration tissues (2010)
18. Usson, Y., Parazza, F., Jouk, P.-S., Michalowicz: Method for the study of the three dimensional orientation of the nuclei of myocardial cells in fetal human heart by means confocal scanning laser microscopy. Journal of Microscopy 174(pt. 2), 101–110 (1994)
19. Walter, et al.: Polarized light microscopy
20. Brehat, F., Wyncke, B.: Répresentation des états de polarisation des ondes lumineuses (2003)
21. Methods for mapping of the orientation of myocardial cells by means of polarized light. Assessment by confocal scanning laser microscopy